Accepted Manuscript

Near-infrared light activation of quenched liposomal Ce6 for synergistic cancer phototherapy with effective skin protection

Liangzhu Feng, Danlei Tao, Ziliang Dong, Qian Chen, Yu Chao, Zhuang Liu, Meiwan Chen

PII: S0142-9612(16)30645-7

DOI: 10.1016/j.biomaterials.2016.11.027

Reference: JBMT 17819

To appear in: *Biomaterials*

Received Date: 16 August 2016

Revised Date: 16 November 2016

Accepted Date: 20 November 2016

Please cite this article as: Feng L, Tao D, Dong Z, Chen Q, Chao Y, Liu Z, Chen M, Near-infrared light activation of quenched liposomal Ce6 for synergistic cancer phototherapy with effective skin protection, *Biomaterials* (2016), doi: 10.1016/j.biomaterials.2016.11.027.

Near-infrared Light Activation of Quenched Liposomal Ce6 for Synergistic Cancer Phototherapy with Effective Skin Protection

Liangzhu Feng[1], Danlei Tao[2], Ziliang Dong[2], Qian Chen[2], Yu Chao[2], Zhuang Liu[2], Meiwan Chen[1]**

Dr. L. Z. Feng, Prof. M. W. Chen
State Key Laboratory of Quality Research in Chinese Medicine, Institute of Chinese Medical Sciences, University of Macau, Macau 999078, China
E-mail: mwchen@umac.mo

Ms. D. L. Tao, Mr. Z. L. Dong, Ms. Q. Chen, Mr. Y. Chao, Prof. Z. Liu
Institute of Functional Nano & Soft Materials (FUNSOM), Jiangsu Key Laboratory for Carbon-Based Functional Materials & Devices, Soochow University, Suzhou 215123, China
E-mail: zliu@suda.edu.cn

Abstract:

Current photodynamic therapy (PDT) is suffering from limited efficacy towards hypoxia tumors and severe post-treatment photo-toxicity such as light-induced skin damages. To make PDT more effective in cancer treatment while being patient-comfortable, herein, a hexylamine conjugated chlorin e6 (*h*Ce6) as the photosensitizer together with a lipophilic near-infrared (NIR) dye 1,1'-dioctadecyl-3,3,3',3'-tetramethylindotricarbocyanine iodide (DiR) are co-encapsulated into polyethylene glycol (PEG) shelled liposomes. In the obtained DiR-*h*Ce6-liposome, the photosensitizing effect of *h*Ce6 is quenched by DiR via fluorescence resonance energy transfer (FRET). Interestingly, upon irradiation with a 785-nm NIR laser to photobleach DiR, both fluorescence and photodynamic effect of *h*Ce6 in DiR-*h*Ce6-liposome would be activated. Meanwhile, such NIR irradiation applied on tumors of mice with intravenous injection of DiR-*h*Ce6-liposome could result in mild photothermal heating, which in turn would promote intra-tumor blood flow and relieve tumor hypoxia, contributing to the enhanced photodynamic tumor treatment. Importantly, compared to *h*Ce6-loaded liposomes, DiR-*h*Ce6-liposome without being activated by the 785-nm laser shows much lower skin photo-toxicity, demonstrating its great skin protection effect. This work demonstrates a promising yet simple strategy to prepare NIR-light-activatable photodynamic theranostics for synergistic cancer phototherapy, which is featured high specificity / efficacy in tumor treatment with minimal photo-toxicity towards the skin.

1. Introduction

Photodynamic therapy (PDT) relies on the singlet oxygen generated from light activated photosensitizers (PSs) to kill diseased cells [1-3]. To date, several different formulations of PSs (e.g. Photofrin® and Visudyne®) have been approved by the food and drug administration (FDA) of USA to treat various diseases including cancers [3-5]. However, as an oxygen-requiring cancer therapy, the therapeutic efficacy of PDT to treat solid tumors is severely affected by the existence of hypoxia in tumors originated from the abnormal tumor growth [3, 6-9]. Moreover, the residual PSs in the skin and eyes post treatment would induce long-lasting photo-toxicity to those tissues / organs even under normal sunlight and indoor lights, significantly reducing the life quality of those patients post PDT [10-12]. Therefore, development of new generation of photodynamic agents and techniques with excellent tumor specificity, the capability to overcome hypoxia-associated resistance in cancer PDT, as well as the minimal post-treatment photo-toxicity, would be of great importance in the development of photodynamic cancer treatment.

With the advance of nanotechnology, a great variety of nano-drug delivery systems (NDDSs) have been extensively explored and found to be promising in improving the bioavailability of many water insoluble drugs including PSs and enhancing their tumor accumulation via the enhanced permeability and retention (EPR) effect, so as to achieve more efficient cancer treatment [13-20]. In recent years, many smart NDDSs responsive to internal or external stimuli (e.g. acidic pH values, redox, enzyme, light) have been developed to improve the selectivity and efficiency of PDT [21-29]. In particular, several different groups including ours have uncovered that modulating tumor

oxygenation levels to relieve tumor hypoxia with smart nano-agents via different approaches (e.g. by in-situ production of oxygen inside the tumor, or improve blood oxygen delivery into tumors) would be able to improve the treatment efficacy of PDT [30-35]. However, although superior tumor specific treatment outcomes have been demonstrated in those studies, how to reduce the photo-toxicity of those newly developed photodynamic nano-agents to healthy tissues such as skin remains a largely unexplored issue to our best knowledge.

Therefore, in this study, a near-infrared (NIR) light activatable liposomal Ce6 agent with efficient skin protection is constructed by simply co-encapsulating *h*Ce6 and DiR molecules into the bilayers of polyethylene glycol (PEG) shelled liposomes (**Figure 1**). It is demonstrated that the as-prepared DiR-*h*Ce6-liposome shows remarkably reduced Ce6 fluorescence, singlet oxygen generation and cell killing ability owing to fluorescence resonance energy transfer (FRET) from *h*Ce6 to DiR with strong NIR absorbance. Interestingly, after NIR irradiation with a 785-nm laser to photo-bleach DiR, the fluorescence as well as singlet oxygen generation capability of *h*Ce6 at its quenched status in such DiR-*h*Ce6-liposome would be efficiently recovered. Therefore, with DiR-*h*Ce6-liposome as an NIR-activatable photodynamic agent, we can use a 785-nm NIR laser with a relatively high laser power density (0.7~1.0 W cm^{-2}) to control PDT triggered by a 660-nm light emitting diode (LED, 2 mW cm^{-2}). In vivo experiments in a mouse tumor model is further carried out. By utilizing the strong absorbance and fluorescence of DiR, the gradual tumor accumulation of DiR-*h*Ce6-liposome after intravenous (i.v.) injection is observed under both photoacoustic (PA) and NIR fluorescence imaging. Notably, the 785-nm laser irradiation locally

applied on the tumor would not only activate *h*Ce6 as evidenced by its recovered fluorescence, but also lead to a mild photothermal heating to promote intra-tumor blood flow and relieve tumor hypoxia, ultimately resulting in a superior synergistic therapeutic effect during in vivo phototherapy of tumors with DiR-*h*Ce6-liposome. Furthermore, a detailed in vivo evaluation of photo-toxicity of DiR-*h*Ce6-liposome is carried out. Compared to *h*Ce6-liposome which results in significant skin photo-toxicity, DiR-*h*Ce6-liposome induces no appreciable photo-toxicity to treated mice at the tested doses. This study demonstrates an innovative yet simple approach to construct an NIR-activatable photodynamic agent with high therapeutic selectivity / efficacy together with minimized photo-toxicity to healthy tissues such as skin.

2. Materials and methods

2.1 Materials

Ce6 was purchased from Frontier Scientific, Inc. 1,2-dipalmitoyl-snglycero-3-phosphocholine (DPPC) was purchased from Xi'an ruixi Biological Technology Co., Ltd. PEG-5000 conjugated 1,2-distearoyl-sn-glycero-3-phosphoethanolamine (DSPE-mPEG$_{5k}$) was purchased from Laysan Bio Inc. DiR was purchased from AAT Bioquest Inc. Cholesterol was purchased from *J&K* Scientific Ltd. Hexylamine, N-(3-Dimethylaminopropyl)-N-ethylcarbodiimide hydrochloride crystalline (EDC), N-Hydroxysuccinimide (NHS), and 3-(4,5-dimethylthiazol-2-yl)-2,5-diphenyl-tetrazolium bromide (MTT) were all purchased from

Sigma-Aldrich. All other chemicals were purchased from China National Pharmaceutical Group Corporation. RPMI-1640 medium and fetal bovine serum (FBS) were purchased from Thermo Fisher Scientific Inc.

2.2 Synthesis of hCe6

*h*Ce6 was prepared by conjugating commercial Ce6 with hexylamine in the presence of EDC and NHS. Briefly, Ce6 (100 mg, 0.17 mmol), hexylamine (88 μL, 0.68 mmol), EDC (132 mg, 0.68 mmol), NHS (77 mg, 0.68 mmol) and trimethylamine (TEA, 95 μL, 0.68 mmol) were dissolved in 10 mL anhydrous dichloromethane and stirred at room temperature for 24 h. Afterwards, the reaction mixture was condensed by rotary evaporation and then purified by thin layer chromatography (TLC) using a mixture of dichloromethane / ethyl acetate (1 : 2, v/v) as the solvent system (RF, 0.7). Afterwards, the individual band was scraped, dispersed with methanol and centrifuged to collect the supernatant. The successful synthesis of *h*Ce6 was confirmed by the matrix-assisted laser desorption / ionization time of flight mass spectrometry (MALDI-TOF MS) and high performance liquid chromatography (HPLC) (Figure S1, supporting information).

2.3 Liposome preparation

To prepare DiR-*h*Ce6-liposome, the lipid mixture of DPPC, cholesterol, DSPE-mPEG$_{5k}$, *h*Ce6 and DiR at a molar ratio of 6 : 4 : 0.5 : 0.5 : 0.5 was dissolved in chloroform and then dried under a rotary evaporator. Afterwards, the dried lipid film was hydrated with phosphate buffered saline

(PBS) and stirred at 45 ^{o}C for 30 min, followed by extruded through a 200 nm polycarbonate filters at 45 °C for 20 times. The obtained DiR-*h*Ce6-liposome was condensed with an Amico filter device with a molecule weight cut-off (MWCO) of 100 kDa (Millipore, Bedford, MA) for further use.

For *h*Ce6-liposome, it was prepared with the same procedure adopted for the preparation of DiR-*h*Ce6-liposome just without the addition of DiR. The size distribution, absorbance and fluorescence spectra of DiR-*h*Ce6-liposome and *h*Ce6-liposome were recorded using a Malvern zetasizer (nano-ZS90), a UV-vis-NIR spectrometer (Thermo Fisher), and a FluoroMax 4 luminescence spectrometer (HORIBA Jobin Yvon), respectively. The morphology of DiR-*h*Ce6-liposome stained by phosphotungstic acid (1 wt.%) was observed under transmission electron microscopy (TEM, Tecnai F20, FEI). The concentrations of DiR and *h*Ce6 were quantified using their absorbance at 760 nm and 664 nm with mass extinction coefficient of 196.3 mL mg^{-1} cm^{-1} and 45.9 mL mg^{-1} cm^{-1}, respectively.

2.4 *Characterization of DiR-hCe6-liposome with 785-nm laser irradiation*

DiR-*h*Ce6-liposome at a DiR concentration of 20 μg mL^{-1} was subjected to a 785-nm laser for 10 min at a power density of 1 W cm^{-2}. Then, the size distribution, absorbance and fluorescence spectra of the irradiated DiR-*h*Ce6-liposome were recorded using the same parameters as those mentioned above. Moreover, the absorbance and fluorescence spectra of *h*Ce6-liposome after exposure to 785-nm laser irradiation at 1 W cm^{-2} for 10 min were also measured under the same parameter settings.

2.5 Evaluation of the singlet oxygen generation ability of DiR-hCe6-liposome

The solutions of DiR-*h*Ce6-liposome with and without 785-nm laser irradiation, *h*Ce6-liposome and free Ce6 at a Ce6 concentration of 5 μM were mixed with SOSG at a final concentration of 2.5 μM in PBS and then subjected to irradiation by a 660-nm LED light at 2 mW cm^{-2}. At 5, 15 and 30 min p.i., 100 μL sample was pipetted out from each well and their fluorescence intensities were recorded using a multimode microreader (Varioskan Flash, Thermo Fisher).

2.6 Cellular uptake of DiR-hCe6-liposome

4T1 murine breast cancer cells was ordered from American Type Culture Collection (ATCC) and maintained according to the recommended procedure. For flow cytometric analysis, 4T1 cells were seeded in a 12-well plate at a density of 8×10^4 cells per well and incubated at 37 ^oC for 24 h. Then, the cells were incubated with fresh medium containing DiR-*h*Ce6-liposome with and without 785-nm laser pre-irradiation (1 W cm^{-2} for 10 min), *h*Ce6-liposome, and free Ce6 at a Ce6 concentration of 5 μM for another 2 h. After that, the medium was removed from the plate and cells were then washed twice with ice-cold PBS, trypsinized, collected, and analyzed using a BD Calibur flow cytometer.

For confocal laser scanning microscopy (CLSM) observation, 4T1 cells were seeded in a 24-well plate containing circle glass coverslides at a density of 3×10^4 cells per well. After being

incubated at 37 ^{o}C for 24 h, the cells were cultured with fresh medium containing DiR-*h*Ce6-liposome with and without 785-nm laser pre-irradiation (1 W cm^{-2} for 10 min), *h*Ce6-liposome, and free Ce6 at a Ce6 concentration of 5 μM for another 2 h. Then, the cells were washed twice with PBS, fixed with 4% paraformalclehyde solution, stained with 4,6-diamino-2-phenyl indole (DAPI), and then imaged under the CLSM (Leica TCS-SP5II, Germany).

2.7 *Cytotoxicity of DiR-hCe6-liposome*

The NIR light activatable cytotoxicity and dark toxicity of DiR-*h*Ce6-liposome were evaluated on 4T1 cells by utilizing the standard MTT assay. Briefly, 4T1 cells were seeded in the 96-well plate at a density of 1 × 10^{4} cells per well and incubated at 37 ^{o}C for 24 h. Then, fresh medium containing DiR-*h*Ce6-liposome with and without 785-nm laser pre-irradiation (1 W cm^{-2} for 10 min), *h*Ce6-liposome, and free Ce6 of various concentrations were added to corresponding wells and incubated for 2 h at 37 ^{o}C. Afterwards, the medium containing materials were removed from the wells and cells were then washed twice with PBS and re-cultured in fresh medium before being irradiated with the 660-nm LED light at 2 mW cm^{-2} for 15 min. Another 22 h later, 25 μL of MTT stock solution (5 mg mL^{-1}) was added into each well and then incubated with cells at 37 ^{o}C for 4 h before discarding the medium and dissolving the formazan by adding 150 μL DMSO. Finally, the absorbance of each well at 570 nm was recorded by a microreader (Model 680, Bio-Rad) to determine the relative cell viabilities.

The dark toxicity of DiR-*h*Ce6-liposome was evaluated according to the same procedure as aforementioned for determining the NIR light activatable cytotoxicity of DiR-*h*Ce6-liposome apart from the cells were not irradiated with the 660-nm LED light.

2.8 In vivo NIR fluorescence and PA imaging of DiR-hCe6-liposome:

Female Balb/c mice and Balb/c nude mice of 18~20 g were purchased from Nanjing Sikerui Biological Technology Co. Ltd. and used under protocols approved by the laboratory animal center of Soochow University. To build the 4T1 tumor model, 2×10^6 4T1 cells in 50 μL PBS were subcutaneously injected to the back of each mouse.

For NIR fluorescence imaging, mice with tumor sizes of ~100 mm^3 were i.v. injected with DiR-*h*Ce6-liposome at a dose of 3.5 mg kg^{-1} body weight (in terms of Ce6). At 1 h, 2 h, 4 h, 8 h and 24 h p.i., the mice was anesthetized and imaged under a Maestro in vivo optical imaging system (Cambridge Research & Instrumentation, Inc) with excitation at 735 nm.

For PA imaging, those tumor-bearing mice were anesthetized and then injected with DiR-*h*Ce6-liposome at dose of 3.5 mg kg^{-1} body weight (in terms of *h*Ce6). Then, at 5 min, 15 min, 30 min, 1 h, 2 h, 4 h and 24 h p.i., the tumor region was imaged using the Visualsonic Vevo® 2100 LAZER system with an excitation wavelength at 700 nm.

2.9 In vivo pharmacokinetics of DiR-hCe6-liposome

To explore the blood circulation profile of DiR-*h*Ce6-liposome, DiR-*h*Ce6-liposome at a dose of 3.5 mg kg^{-1} body weight (in terms of *h*Ce6) was i.v. injected to three healthy Balb/c mice. At different time intervals, ~20 μL blood was taken out from each mouse and then lysed with blood lysis buffer containing 1% sodium dodecylsulfate (SDS), 1% Triton X-100, 40 mM tris(hydroxymethyl)aminomethane (tris) acetate, 10 mM ethylenediaminetetraacetic acid (EDTA), 10 mM dithiothreitol (DTT). Then, the fluorescence intensity of each sample was recorded using the Varioskan Flash multimode microreader.

For analyzing the biodistribution profile of DiR-*h*Ce6-liposome, three 4T1 tumor bearing mice with a tumor size of ~100 mm^3 received i.v. injection of DiR-*h*Ce6-liposome at a dose of 3.5 mg kg^{-1} body weight (in terms of *h*Ce6). At 24 h p.i., the mice were sacrificed and main organs/tissues including liver, spleen, kidney, heart, lung, stomach, intestine, skin, muscle and tumor were then collected and homogenized in 1 mL lysis buffer with a Fluko homogenizer. Afterwards, the fluorescence intensity of each sample after appropriate dilution was recorded using the Varioskan Flash multimode microreader.

2.10 In vivo NIR laser induced activation of DiR-hCe6-liposome

The capability of the 785-nm NIR laser irradiation to activate DiR-*h*Ce6-liposme in vivo inside the tumor was evaluated using a Maestro in vivo optical imaging system. 3 female Balb/c nude mice bearing 4T1 tumor of ~100 mm^3 were i.v. injected with DiR-*h*Ce6-liposome at a dose of 3.5 mg kg^{-1} body weight in terms of Ce6. 24 h later, the mice were anesthetized and imaged under

523-nm and 735-nm excitations to collect fluorescence signals of *h*Ce6 and DiR, respectively. Then, the tumors were exposed to a 785-nm laser at a power density of ~0.7 W cm^{-2}. The tumor temperature was maintained at ~45 ^{o}C as recorded using a NIR thermal camera (Fotric 225) throughout the 20-min laser irradiation. Afterwards, the mice were imaged again under the aforementioned parameter settings. Finally, the fluorescence emission at 660 nm under 523 nm excitation (*h*Ce6 fluorescence) and that at 800 nm under 735 nm excitation (DiR fluorescence) from the tumor before and after 785-nm laser irradiation were quantified in order to determine how such NIR laser irradiation would activate DiR-*h*Ce6-liposome in the tumor.

2.11 Evaluation of tumor oxygenation

For ex vivo immunofluorescence staining to evaluate the tumor hypoxia status, 4T1 tumor-bearing with i.v. injection of DiR-*h*Ce6-liposome (*h*Ce6 dose = 3.5 mg kg^{-1}) were irradiated with a 785-nm laser at ~0.7 W cm^{-2} for 20 min at 24 h p.i. In the meanwhile, mice with i.v. injection of DiR-*h*Ce6-liposome but without laser irradiation were used as the control. Then, the mice were intraperitoneally injected with pimonidazole hydrochloride (Hypoxyprobe^{TM}, USA) at a dose of 30 mg kg^{-1} according to the procedure provided by the manufacturer. After 90 min, those mice were sacrificed to collect frozen tumor slices, which were firstly stained with a mixture of anti-pimonidazole mouse monoclonal antibody and rat-anti-mouse CD31 antibody as primary antibodies for tumor hypoxia region and blood vessels, respectively, and then stained with Alexa

Fluo 488 conjugated goat-anti-mouse antibody and rhodamine conjugated donkey-anti-rat antibody as secondary antibodies.

2.12 In vivo combination therapy with DiR-hCe6-liposome

30 female Balb/c mice bearing 4T1 tumors were randomly divided to 5 groups. When the tumor sizes reached ~100 mm^3, two groups of those mice were i.v. injected with saline or *h*Ce6-liposome, while the other three groups of mice were i.v. injected with DiR-*h*Ce6-liposome at the same *h*Ce6 dose (3.5 mg kg^{-1}). At 24 h p.i., *h*Ce6-liposome injected mice and one group of DiR-*h*Ce6-liposome injected mice were irradiated with a 660-nm LED light at a power density of 2 mW cm^{-2}. Another group of DiR-*h*Ce6-liposome injected mice were irradiated with a 785-nm laser for 20 min with the tumor temperature kept at ~45 ^oC during laser irradiation. The third group of DiR-*h*Ce6-liposome injected mice were firstly photothermally heated at ~45 ^oC using a 785-nm laser for 20 min and then followed by 1-h irradiation with the 660-nm LED light.

The tumor length and width of each mouse were recorded using a digital caliper every two days since the beginning of the treatment. The tumor volume (*V*) was calculated following the equation: $V = LW^2/2$, in which *L* and *W* refer to the length and width of the tumor in millimeters, respectively. In addition, the body weight of each mouse was also measured using a digital balance every the other day. At day 14 post treatment, the mice were sacrificed and their tumors were collected for weighing. Moreover, the main organs including liver, spleen, kidney, heart and lung of saline injected control group and DiR-*h*Ce6-liposome injected combination therapy group were

collected, fixed using 4% paraformalclehyde solution, mounted with paraffine, sliced, stained with H&E, and then imaged using a microscopy. To evaluate the therapeutic effects of those different treatments, one mouse from each group was sacrificed 1 day post laser irradiation, with its tumor collected and split into two halves for hematoxylin and eosin (H&E) staining and terminal deoxynucleotidyl transferase dUTP nick end labeling (TUNEL) assay, respectively.

2.13 In vivo photo-toxicity of DiR-hCe6-liposome

To evaluate the in vivo photo-toxicity of DiR-*h*Ce6-liposome in comparison to *h*Ce6-liposome, 50 healthy female mice with hair removed were randomly divided to 5 groups, with 5 mice of each group used for recording the body weight and the other 5 mice used for other evaluations. Two groups of mice were i.v. injected with DiR-*h*Ce6-liposome at *h*Ce6 doses of 1.75 mg kg^{-1} and 3.5 mg kg^{-1}, while the other two groups were i.v. injected with *h*Ce6-liposome at the same *h*Ce6 doses. At 4 h p.i., the all mice were exposed to a 660-nm LED light at a power density of 2 mW cm^{-2} for 30 min. At 4 h, 2 days and 8 days post treatment, the mice from each group were imaged with a digital camera. Besides, three mice of each group were sacrificed to collect the skin on their back of with the exact size of 1.5 cm × 1.5 cm for weighing at 4 h post treatment. H&E staining was also conducted following the previously mentioned protocol to evaluate light-induced skin damage. Moreover, the body weight of each mouse was recorded using a digital balance for 8 days since the beginning of experiments.

3. Results and discussion

In this work, a commercial lipophilic DiR molecule with strong NIR absorbance and fluorescence, together with the modified *h*Ce6 (by conjugating one Ce6 with three hexylamine to increase its hydrophobicity, see method section for details), were co-capsulated into PEGylated liposomes. In brief, DiR-*h*Ce6-liposome was prepared by mixing DPPC, cholesterol, DSPE-mPEG$_{5k}$, *h*Ce6 and DiR at a molar ratio of 6 : 4 : 0.5 : 0.5 : 0.5 according to standard method for preparation of liposomes. As expected, DiR-*h*Ce6-liposome showed characteristic peaks of DiR and *h*Ce6 at 760 nm and 404 nm, respectively, on its UV-vis-NIR absorbance spectrum (**Figure 2a**). The other *h*Ce6 characteristic peak shown in *h*Ce6-liposome at ~670 nm overlaid significantly with the DiR absorbance peak. Dynamic light scattering (DLS) measurement revealed the average size of DiR-*h*Ce6-liposome to be ~150 nm, which was similar to that of its counterpart *h*Ce6-liposome prepared by adopting the same procedure used for DiR-*h*Ce6-liposome but in the absence of DiR (**Figure 2b**). Under TEM, the obtained DiR-*h*Ce6-liposome showed uniform sphere-like morphology (**Figure S2**). Moreover, owning to the presence of DiR, the fluorescence of *h*Ce6 in DiR-*h*Ce6-liposme was quenched by ~97% in comparison with that of *h*Ce6-liposome at the same *h*Ce6 concentration due to FRET. Such a high FRET efficiency might be attributed to the high packing density of DiR and *h*Ce6 in the bilayers of liposomes, as well as the large overlap between *h*Ce6 emission and DiR absorbance peaks. (**Figure 2c**).

Then, the effects of 785-nm laser irradiation on the optical properties of DiR-*h*Ce6-liposome were carefully examined. After being exposed to a 785-nm laser for 10 min at 1 W cm^{-2}, the DiR

absorbance in DiR-*h*Ce6-liposome at 760 nm dropped by ~95% due to the poor photo-stability of DiR similar to many other organic small dye molecules (**Figure 2a**) [36]. Meanwhile, it was found that the fluorescence of *h*Ce6 in DiR-*h*Ce6-liposome after 785-nm laser irradiation remarkably recovered, owing to the diminished quenching effect of DiR to *h*Ce6 after photobleaching of the former one (**Figure 2c**). In comparison, such a laser irradiation has minimal influence on the absorbance and fluorescence properties of *h*Ce6-liposome (**Figure S3**), which has no optical absorbance at 785 nm. Though obvious changes in optical properties were observed when DiR-*h*Ce6-liposome was irradiated by the 785-nm laser, little fluctuation on its size distribution was noted by the DLS measurement (**Figure 2b**), indicating the great structural stability of DiR-*h*Ce6-lipsome during laser irradiation. Afterwards, the in vitro singlet oxygen generation abilities of DiR-*h*Ce6-liposome before and after exposure to the 785-nm laser irradiation, as well as *h*Ce6-liposome and free Ce6 molecules at the same Ce6 concentration, were measured under exposure to 660-nm LED light (2 mW cm^{-2} for 30 min) using a commercial singlet oxygen sensor green (SOSG) kit (**Figure 2d**). It was found that the singlet oxygen generation ability of DiR-*h*Ce6-liposome was only ~18% and ~16% to those of *h*Ce6-liposome and free Ce6, respectively, indicating that the photosensitizing ability of *h*Ce6 in DiR-*h*Ce6-liposome was efficiently quenched by DiR via FRET. In contrast, for DiR-*h*Ce6-liposome after activation by the 785-nm laser to photobleach DiR, its 660-nm light-induced singlet oxygen generation would be significantly recovered, to ~90% and ~77% compared to that of plain *h*Ce6-liposome and free Ce6, respectively. Taken together, those results indicate that the photodynamic effect of such

DiR-*h*Ce6-liposome at its quenched state would be activated under exposure to the 785-nm NIR laser.

Next, we evaluated NIR-activated PDT with DiR-*h*Ce6-liposome at the cellular level in our carefully designed in vitro experiments. 4T1 murine breast cancer cells were incubated with DiR-*h*Ce6-liposome, *h*Ce6-liposome or free Ce6 for 2 h, and then examined by flow cytometry and CLSM. Flow cytometry measurement uncovered that cells incubated with DiR-*h*Ce6-liposome showed rather weak Ce6 signals. However, for those cells incubated with the DiR-*h*Ce6-liposome that was pre-irradiated with the 785-nm laser (1 W cm^{-2} for 10 min), the cellular Ce6 fluorescence signals were remarkably recovered, reaching a level as high as that for cells incubated with plain *h*Ce6-liposome. In addition, though free Ce6 had a strong fluorescence, free Ce6 treated cells showed weak fluorescence signals, probably attributing to the inefficient cellular uptake of free Ce6 molecules (**Figure 3a**). Besides, CLSM observation showed similar results to those obtained by flow cytometric analysis (**Figure 3b**). Strong Ce6 fluorescence signals inside cells were observed for cells incubated with DiR-*h*Ce6-liposome only after it was pre-activated by the 785-nm NIR laser.

Afterwards, the standard cell viability assay was conducted for cells incubated with various formulations of Ce6 after phototherapy. Owing to the quenching effect of DiR in DiR-*h*Ce6-liposome, minor photo-toxicity was observed on those cells treated with DiR-*h*Ce6-liposome incubation plus 660-nm light exposure at the tested doses. In contrast, significantly improved cell killing ability of DiR-*h*Ce6-liposome was observed upon the

photobleaching of DiR using the 785-nm laser (1 W cm^{-2} for 10 min) before incubation with cells, reaching a photodynamic cell killing effect comparable to that of plain *h*Ce6-liposome. Additionally, owing to the less efficient cellular uptake as observed previously (**Figure 3a&b**), free Ce6 showed relatively weak cytotoxicity to the treated cells under the same experimental conditions (**Figure 3c**). Furthermore, DiR-*h*Ce6-liposome, *h*Ce6-liposome and free Ce6 at the same concentrations without 660-nm LED light irradiation showed negligible effect on the cell viability (**Figure 3d**), indicating little dark toxicity of those agents. Collectively, those in vitro evaluations demonstrate such DiR-*h*Ce6-liposome to be a NIR light activatable nano-PS that could be turn on by photobleaching of the quenching molecule, DiR.

Motivated by those exciting in vitro results, the in vivo performance of DiR-*h*Ce6-liposome was carefully studied. Utilizing the strong NIR absorbance and fluorescence of DiR, in vivo fluorescence and PA imaging were conducted to track the in vivo accumulation of DiR-*h*Ce6-liposome in 4T1 tumors grown on Balb/c mice post intravenous (i.v.) injection. Under in vivo fluorescence imaging, gradually increased DiR fluorescence signals in the tumor were visualized following i.v. injection of DiR-*h*Ce6-liposome (**Figure 4a&S5**), similar to our previously reported results [37]. Considering that PA imaging could offer superior tissue penetration and excellent in vivo spatial resolution over conventional in vivo fluorescence imaging [12, 38, 39], we further studied the tumor accumulation profile of DiR-*h*Ce6-liposome in 4T1 tumor bearing mice with PA imaging, which also revealed gradually increased tumor accumulation of DiR-*h*Ce6-liposome (**Figure 4b**). More interestingly, it was found that DiR-*h*Ce6-liposome would

firstly perfuse the peripheral regions of tumor at 5 min post injection (p.i.) and then increasingly defuse throughout the whole tumor. This intriguing distribution pattern might be correlated with the intra-tumor heterogeneous distribution of blood vessels. Our results collectively evidenced the excellent tumor homing ability of such DiR-*h*Ce6-liposome.

Furthermore, quantitative in vivo blood circulation and biodistribution of DiR-*h*Ce6-liposome were determined by utilizing the strong NIR fluorescence of DiR. By measuring the DiR fluorescence intensities of each blood sample collected from healthy mice with i.v. injection of DiR-*h*Ce6-liposome at different time intervals, it was found that DiR-*h*Ce6-liposome followed a two-compartment model during its systemic blood circulation, with its first half-life time ($t_{1/2(\alpha)}$) and second half-life time ($t_{1/2(\beta)}$) measured to be 1.6 ± 0.44 h and 10.3 ± 2.3 h, respectively (**Figure 4c**). In addition, 4T1 tumor bearing mice with i.v. injection of DiR-*h*Ce6-liposome were sacrificed at 24 h p.i. Their main organs and tissues were collected and homogenized for measuring the DiR fluorescence intensity. The reticuloendothelial system (RES) including liver and spleen had high accumulation of DiR-*h*Ce6-liposome, similar to many other NDDSs [40]. Meanwhile, the tumor accumulation reached 6.84 ± 0.32 ID% g^{-1} (percentage of injected dose per gram tissue) (**Figure 4d**). All those results indicate that the excellent stealth-like blood circulation profile and high passive tumor accumulation of such DiR-*h*Ce6-liposome.

Inspired by the in vitro results that the quenched photosensitizing ability of DiR-*h*Ce6-liposome could be efficiently recovered by photobleaching DiR using the 785-nm NIR laser, we herein wondered if its in vivo photosensitizing activity could be recovered by the same

way, thereby conferring tumor specific PDT. To avoid direct photothermal ablation of tumors, the temperature of those 4T1 tumors on mice injected with DiR-*h*Ce6-liposome was monitored using an infrared thermal camera and kept around 45 ^{o}C during irradiation by the 785-nm laser at 0.7-1.0 W cm^{-2} for 20 min for the activation of DiR-*h*Ce6-liposome (**Figure 5a&b**). As expected, it was found that the DiR fluorescence (excitation = 735 nm, emission = 800 nm) on tumors of mice with DiR-*h*Ce6-liposome injection was significantly quenched after irradiation by the 785-nm laser for 20 min (**Figure 5c&d**). More excitingly, the fluorescence of *h*Ce6 (excitation = 523 nm, emission = 660 nm), which was excited by a shorter wavelength light source to avoid interference of DiR fluorescence, showed about two times enhancement on tumors of DiR-*h*Ce6-liposome injected mice after DiR was photobleached by the tumor-focused 785-nm laser. Those results collectively demonstrate that the mild 785-nm laser irradiation is a promising strategy to activate DiR-*h*Ce6-liposome, making it selectively works at the tumor site.

In previous studies, it has been reported that pretreatment of tumors with a mild hyperthermia could effectively oxygenate tumors, making them more susceptible to various treatment modalities including PDT [41-45]. Therefore, by utilizing ex vivo immunofluorescence staining with the pimonidazole as the hypoxia staining probe, it was found that 4T1 tumors without laser irradiation showed severe hypoxia, which however could be significantly relieved after laser irradiation (**Figure 5e**). Semi-quantitative analysis of hypoxia-positive signals in those tumor slices uncovered that the percentage of hypoxia-positive area dramatically dropped from ~38% to only ~12% for those after the mild NIR-induced photothermal heating with DiR-*h*Ce6-liposome (**Figure 5f**). Those

results indicate that such mild photothermal effect is efficient in modulating the tumor oxygenation, promising for improving the treatment outcomes of PDT since oxygen is a determinant factor for efficient PDT [4].

After that, the in vivo NIR light activatable tumor specific therapeutic effects of DiR-*h*Ce6-liposome were evaluated using 4T1 tumor-bearing mice. 30 female Balb/c mice bearing 4T1 tumors with sizes ~100 mm^3 were randomly divided into 5 groups as follows: I) control group by saline injection only; II) conventional PDT group by *h*Ce6-liposome injection plus 660-nm LED light exposure (2 mW cm^{-2} for 1 h) at 24 h p.i.; III) quenched PDT group by DiR-*h*Ce6-liposome injection plus 660-nm LED light exposure (2 mW cm^{-2} for 1 h) at 24 h p.i.; IV) mild photothermal heating group by DiR-*h*Ce6-liposome injection plus tumor-specific 785-nm laser irradiation (0.7 W cm^{-2} for 20 min, with the tumor temperature maintained at ~45 ^oC) at 24 h p.i.; and V) activated PDT group by DiR-*h*Ce6-liposome injection plus sequential 785-nm laser irradiation (0.7 W cm^{-2} for 20 min) and 660-nm LED light exposure (2 mW cm^{-2} for 1 h) at 24 h p.i. The Ce6 dose was 3.5 mg kg^{-1} in all related groups. Then, the tumor sizes on each group of mice were recorded using a digital caliper. It was observed that the tumor growth of those injected with DiR-*h*Ce6-liposome followed by sequential irradiation of 785-nm laser and 660-nm LED light was remarkably regressed, while treatment of *h*Ce6-liposome injection plus 660-nm LED light irradiation (conventional PDT) only showed a moderate tumor growth inhibition effect on those treated mice. On the contrary, the tumor growth was not obviously disturbed by the treatments of DiR-*h*Ce6-liposome injection plus either bare 785-nm laser (mild photothermal heating) or 660-nm LED light irradiation (quenched

PDT), suggesting that mild photothermal heating at this temperature was not able to delay the tumor growth, DiR-*h*Ce6-liposome without activation by the 785-nm laser was an ineffective PDT agent (**Figure 6a**). Moreover, similar results were obtained by weighting the tumors collected from each treated group of mice at 14 days p.i. (**Figure 6b**). In comparison with the predicted additive effect by multiplying the tumor growth inhibition ratios of conventional PDT group and mild photothermal heating group, the treatment outcome of the activated PDT group appeared to be much more effective, indicating that our developed strategy would exhibit promising synergistic treatment effect over those mono-therapies.

To further confirm the therapeutic effect, both H&E staining and TUNEL assay were utilized to analyze histological changes and apoptosis levels of tumors, respectively, at 24 h post various treatments. From H&E staining, severe morphology change and necrosis were observed for tumors treated with DiR-*h*Ce6-liposome injection plus sequential 785-nm laser (activation) and 660-nm light (PDT) irradiation, while only moderate damage was observed for tumors of mice post PDT with *h*Ce6-liposome, and negligible tumor damage was noted for other control groups of mice (**Figure 6c**). The apoptosis levels in tumors revealed by TUNEL assay followed the same trend (**Figure 6d**). Taken together, those results indicate that such DiR-*h*Ce6-liposome is a promising candidate for NIR light activatable synergistic cancer therapy, in which the tumor-focused 785-nm laser irradiation could selectively activate the photodynamic effect of DiR-*h*Ce6-liposome accumulated in the tumor, meanwhile the mild photothermal heating could efficiently relieve the tumor hypoxia to further improve the therapeutic effect of PDT.

Motivated by the aforementioned in vivo cancer treatment results indicating that DiR-*h*Ce6-liposome would not show obvious photodynamic effect until DiR is photobleached, we wondered if such DiR-*h*Ce6-liposome would exhibit reduced photo-toxicity to the skin, which is often damaged during conventional PDT. Therefore, the photo-toxicity of DiR-*h*Ce6-liposome was evaluated on mouse skin in comparison with that of plain *h*Ce6-liposome as the example of conventional PDT to demonstrate the skin protection ability of DiR-*h*Ce6-liposome according to previously reported methods [46-49]. Healthy female Balb/c mice with hair removed were randomly divided to 5 groups: saline control, DiR-*h*Ce6-liposome injection with two different *h*Ce6 doses (1.75 mg kg^{-1} or 3.5 mg kg^{-1}), and *h*Ce6-liposome injection with two different *h*Ce6 doses (1.75 mg kg^{-1} or 3.5 mg kg^{-1}). All mice were exposed to the 660-nm LED light (2 mW cm^{-2} for 30 min) at 4 h p.i. While obvious edema was observed on the back of *h*Ce6-liposome injected mice post light exposure (**Figure 7a**), mice receiving injection of DiR-*h*Ce6-liposome showed no appreciable skin side effect after light irradiation. To quantitatively compare the edema of mice with different treatments, three piece of skin at 1.5 cm × 1.5 cm were taken from the back of three sacrificed mice of each group and then weighted at 4 h post light irradiation. It was uncovered that the skin weight of mice injected with DiR-*h*Ce6-liposome after light exposure showed negligible difference compared to the saline control, while the skin weights of *h*Ce6-liposome treated mice showed significant increases upon light exposure (**Figure 7b**). At 24 h post irradiation, the edema would gradually disappeared (data not shown), while obvious erythema and eschar were formed on the back of mice treated with *h*Ce6-liposome at 3.5 mg kg^{-1} body weight at 2 days post irradiation.

Such dose-dependent sign of skin damage induced by *h*Ce6-liposome would not disappear until 8 days post light irradiation (**Figure 7a**).

We further carried out a careful histology examination of skins collected from different groups of mice by H&E staining at 2 days post irradiation. It was found that the skins of DiR-*h*Ce6-liposome treated mice remained intact as that of saline control mice post light exposure. In remarkable contrast, epidermis of those treated with *h*Ce6-liposome was much thinner than that of saline control group, and obvious necrosis was observed in the region of dermis (**Figure 7d**). Furthermore, the body weights of different treated groups of mice were recorded for 8 days. It was found that mice treated with *h*Ce6-liposome of 3.5 mg kg^{-1} after light exposure showed obvious body weight loss, which was not observed for DiR-*h*Ce6-liposome injected mice after light exposure at the same *h*Ce6 and optical doses (**Figure 7c**). All these results collectively demonstrate that our DiR-*h*Ce6-liposome is promising in diminishing the severe photo-toxicity of conventional PDT, highlighting a meaningful strategy in designing new generation of nano-PSs with excellent selectivity, efficacy and safety.

4. Conclusion

In this study, we designed NIR light activatable liposomal Ce6 and then explored its capacity for cancer phototherapy with minimal skin photo-toxicity. Owing to the strong NIR absorbance of DiR, the photosensitizing ability of *h*Ce6 in the obtained DiR-*h*Ce6-liposome was blocked due to FRET, but would be easily recovered by exposure to a 785-nm laser to photobleaching DiR, as

demonstrated in both in vitro and in vivo experiments. Moreover, ex vivo immunofluorescence imaging demonstrated that the mild photothermal effect could efficiently relieve tumor hypoxia, subsequently contributing to an effective synergistic therapeutic effect in cancer PDT. In addition, excellent skin protection ability of DiR-*h*Ce6-liposome was uncovered by evaluating its photo-toxicity to the tested mouse skin. Taken together, such DiR-*h*Ce6-liposome shows several advantages over most of other conventional nano-PSs for the following reasons: 1) its minimal photosensitivity to skin would make it much safer and more comfortable for patients; 2) tumor localized activation would further improve the selectivity of treatment; 3) utilizing the mild photothermal effect to modulating tumor hypoxia would produce a synergistic treatment effect; 4) its excellent biocompatibility and well defined composition would make it much easier for further clinical translation.

Supporting Information

Supplementary data related to this article can be found at …

Acknowledgements

This work was partially supported by the National Research Programs from Ministry of Science and Technology (MOST) of China (2016YFA0201200), the National Natural Science Foundation of China (51525203), a Juangsu Natural Science Fund for Distinguished Young Scholars (BK20130005), Collaborative Innovation Center of Suzhou Nano Science and Technology,

and a Project Funded by the Priority Academic Program Development (PAPD) of Jiangsu Higher Education Institutions, the Macao Science and Technology Development Fund (062/2013/A2), and the Research Fund of the University of Macau (MYRG2014-00033-ICMS-QRCM, MYRG2014-00051-ICMS-QRCM).

References

[1] Dougherty TJ, Gomer CJ, Henderson BW, Jori G, Kessel D, Korbelik M, et al. Photodynamic Therapy. J. Natl. Cancer I. 1998;90:889-905.

[2] Cheng L, Wang C, Feng L, Yang K, Liu Z. Functional Nanomaterials for Phototherapies of Cancer. Chem. Rev. 2014;114:10869-939.

[3] Agostinis P, Berg K, Cengel KA, Foster TH, Girotti AW, Gollnick SO, et al. Photodynamic therapy of cancer: An update. CA. Cancer J. Clin. 2011;61:250-81.

[4] Dolmans DEJGJ, Fukumura D, Jain RK. Photodynamic therapy for cancer. Nat. Rev. Cancer 2003;3:380-7.

[5] Huang Z. A Review of Progress in Clinical Photodynamic Therapy. Technol. Cancer Res. T. 2005;4:283-93.

[6] Vaupel P, Thews O, Hoeckel M. Treatment resistance of solid tumors. Med. Oncol. 2001;18:243-59.

[7] Ji Z, Yang G, Shahzidi S, Tkacz-Stachowska K, Suo Z, Nesland JM, et al. Induction of hypoxia-inducible factor-1α overexpression by cobalt chloride enhances cellular resistance to photodynamic therapy. Cancer Lett. 2006;244:182-9.

[8] Koukourakis MI, Giatromanolaki A, Skarlatos J, Corti L, Blandamura S, Piazza M, et al. Hypoxia Inducible Factor (HIF-1a and HIF-2a) Expression in Early Esophageal Cancer and Response to Photodynamic Therapy and Radiotherapy. Cancer Res. 2001;61:1830-2.

[9] Vaupel P, Mayer A. Hypoxia and anemia: effects on tumor biology and treatment resistance. Transfus. Clin. et Biol. 2005;12:5-10.

[10] Bellnier DA, Greco WR, Nava H, Loewen GM, Oseroff AR, Dougherty TJ. Mild skin photosensitivity in cancer patients following injection of Photochlor (2-[1-hexyloxyethyl]-2-devinyl pyropheophorbide-a; HPPH) for photodynamic therapy. Cancer Chemother. Pharmacol. 2006;57:40-5.

[11] Roberts WG, Smith KM, McCuliough JL, Berns MW. SKIN PHOTOSENSITIVITY AND PHOTODESTRUCTION OF SEVERAL POTENTIAL PHOTODYNAMIC SENSITIZERS. Photochem. Photobiol. 1989;49:431-8.

[12] Vrouenraets MB, Visser GWM, Snow GB, van Dongen GAMS. Basic principles, applications in oncology and improved selectivity of photodynamic therapy. Anticancer Res. 2003;23:505-22.

[13] Torchilin VP. Recent advances with liposomes as pharmaceutical carriers. Nat. Rev. Drug Discov. 2005;4:145-60.

[14] Yang G, Liu J, Wu Y, Feng L, Liu Z. Near-infrared-light responsive nanoscale drug delivery systems for cancer treatment. Coord. Chem. Rev. 2016, DOI:10.1016/j.ccr.2016.04.004

[15] Yang K, Feng L, Shi X, Liu Z. Nano-graphene in biomedicine: theranostic applications. Chem. Soc. Rev. 2013;42:530-47.

[16] Farokhzad OC, Langer R. Impact of Nanotechnology on Drug Delivery. ACS Nano. 2009;3:16-20.

[17] Zhen Z, Tang W, Chuang Y-J, Todd T, Zhang W, Lin X, et al. Tumor Vasculature Targeted

Photodynamic Therapy for Enhanced Delivery of Nanoparticles. ACS Nano. 2014;8:6004-13.
[18] Choi HW, Kim J, Kim J, Kim Y, Song HB, Kim JH, et al. Light-Induced Acid Generation on a Gatekeeper for Smart Nitric Oxide Delivery. ACS Nano. 2016;10:4199-208.
[19] Chuang E-Y, Lin C-C, Chen K-J, Wan D-H, Lin K-J, Ho Y-C, et al. A FRET-guided, NIR-responsive bubble-generating liposomal system for in vivo targeted therapy with spatially and temporally precise controlled release. Biomaterials. 2016;93:48-59.
[20] Wang M, Sun S, Neufeld CI, Perez-Ramirez B, Xu Q. Reactive Oxygen Species-Responsive Protein Modification and Its Intracellular Delivery for Targeted Cancer Therapy. Angew. Chem. Int. Ed. 2014;53:13444-8.
[21] Jang B, Park J-Y, Tung C-H, Kim I-H, Choi Y. Gold Nanorod−Photosensitizer Complex for Near-Infrared Fluorescence Imaging and Photodynamic/Photothermal Therapy In Vivo. ACS Nano. 2011;5:1086-94.
[22] Zheng G, Chen J, Stefflova K, Jarvi M, Li H, Wilson BC. Photodynamic molecular beacon as an activatable photosensitizer based on protease-controlled singlet oxygen quenching and activation. Proc. Natl. Acad. Sci. USA. 2007;104:8989-94.
[23] Lovell JF, Liu TWB, Chen J, Zheng G. Activatable Photosensitizers for Imaging and Therapy. Chemical Reviews. 2010;110:2839-57.
[24] Yang G, Sun X, Liu J, Feng L, Liu Z. Light-Responsive, Singlet Oxygen-Triggered On-Demand Drug Release from Photosensitizer-Doped Mesoporous Silica Nanorods for Cancer Combination Therapy. Adv. Funct. Mater. 2016, DOI: 10.1002/adfm.201600722
[25] Yuan A, Tang X, Qiu X, Jiang K, Wu J, Hu Y. Activatable photodynamic destruction of cancer cells by NIR dye/photosensitizer loaded liposomes. Chem. Commun. 2015;51:3340-2.
[26] Hu D, Sheng Z, Gao G, Siu F, Liu C, Wan Q, et al. Activatable albumin-photosensitizer nanoassemblies for triple-modal imaging and thermal-modulated photodynamic therapy of cancer. Biomaterials. 2016;93:10-9.
[27] Tian B, Wang C, Zhang S, Feng L, Liu Z. Photothermally Enhanced Photodynamic Therapy Delivered by Nano-Graphene Oxide. ACS Nano. 2011;5:7000-9.
[28] Yuan Y, Zhang C-J, Gao M, Zhang R, Tang BZ, Liu B. Specific Light-Up Bioprobe with Aggregation-Induced Emission and Activatable Photoactivity for the Targeted and Image-Guided Photodynamic Ablation of Cancer Cells. A Angew. Chem. Int. Ed. 2015;54:1780-6.
[29] Li W, Zheng C, Pan Z, Chen C, Hu D, Gao G, et al. Smart hyaluronidase-actived theranostic micelles for dual-modal imaging guided photodynamic therapy. Biomaterials. 2016;101:10-9.
[30] Gong H, Chao Y, Xiang J, Han X, Song G, Feng L, et al. Hyaluronidase To Enhance Nanoparticle-Based Photodynamic Tumor Therapy. Nano Lett. 2016;16:2512-21.
[31] Zhu W, Dong Z, Fu T, Liu J, Chen Q, Li Y, et al. Modulation of Hypoxia in Solid Tumor Microenvironment with MnO2 Nanoparticles to Enhance Photodynamic Therapy. Adv. Funct. Mater. 2016, DOI: 10.1002/adfm.201600676.
[32] Fan W, Bu W, Shen B, He Q, Cui Z, Liu Y, et al. Intelligent MnO2 Nanosheets Anchored with Upconversion Nanoprobes for Concurrent pH-/H2O2-Responsive UCL Imaging and Oxygen-Elevated Synergetic Therapy. Adv. Mater. 2015;27:4155-61.

[33] Gordijo CR, Abbasi AZ, Amini MA, Lip HY, Maeda A, Cai P, et al. Design of Hybrid MnO2-Polymer-Lipid Nanoparticles with Tunable Oxygen Generation Rates and Tumor Accumulation for Cancer Treatment. Adv. Funct. Mater.. 2015;25:1858-72.

[34] Fan H, Yan G, Zhao Z, Hu X, Zhang W, Liu H, et al. A Smart Photosensitizer–Manganese Dioxide Nanosystem for Enhanced Photodynamic Therapy by Reducing Glutathione Levels in Cancer Cells. Angew. Chem. Int. Ed. 2016;128:5567-72.

[35] Luo Z, Zheng M, Zhao P, Chen Z, Siu F, Gong P, et al. Self-Monitoring Artificial Red Cells with Sufficient Oxygen Supply for Enhanced Photodynamic Therapy. Sci. Rep. 2016, 6. DOI:10.1038/srep23393.

[36] Song X, Chen Q, Liu Z. Recent advances in the development of organic photothermal nano-agents. Nano Res. 2015;8:340-54.

[37] Feng L, Gao M, Tao D, Chen Q, Wang H, Dong Z, et al. Cisplatin-Prodrug-Constructed Liposomes as a Versatile Theranostic Nanoplatform for Bimodal Imaging Guided Combination Cancer Therapy. Adv. Functi. Mater. 2016;26:2207-17.

[38] Xu M, Wang LV. Photoacoustic imaging in biomedicine. Rev. Sci. Instrum. 2006;77:041101.

[39] Wang LV, Hu S. Photoacoustic Tomography: In Vivo Imaging from Organelles to Organs. Science. 2012;335:1458-62.

[40] Gabizon A, Price DC, Huberty J, Bresalier RS, Papahadjopoulos D. EFFECT OF LIPOSOME COMPOSITION AND OTHER FACTORS ON THE TARGETING OF LIPOSOMES TO EXPERIMENTAL-TUMORS - BIODISTRIBUTION AND IMAGING STUDIES. Cancer Res. 1990;50:6371-8.

[41] Chen Q, Chen H, Shapiro H, Hetzel FW. Sequencing of Combined Hyperthermia and Photodynamic Therapy. Radiat. Res. 1996;146:293-7.

[42] Brizel DM, Scully SP, Harrelson JM, Layfield LJ, Dodge RK, Charles HC, et al. Radiation Therapy and Hyperthermia Improve the Oxygenation of Human Soft Tissue Sarcomas. Cancer Res. 1996;56:5347-50.

[43] Song CW, Rhee JG, Levitt SH. Effect of hyperthermia on hypoxic cell fraction in tumor. Int. J. Radiat. Oncol. Biol. Phys. 1982;8:851-6.

[44] Song G, Liang C, Gong H, Li M, Zheng X, Cheng L, et al. Core–Shell MnSe@Bi2Se3 Fabricated via a Cation Exchange Method as Novel Nanotheranostics for Multimodal Imaging and Synergistic Thermoradiotherapy. Adv. Mater. 2015;27:6110-7.

[45] Gormley AJ, Larson N, Sadekar S, Robinson R, Ray A, Ghandehari H. Guided delivery of polymer therapeutics using plasmonic photothermal therapy. Nano Today. 2012;7:158-67.

[46] Lankerani L, Baron ED. Photosensitivity to Exogenous Agents. J. Cutan. Med. Surg. 2004;8:424-31.

[47] Chin WWL, Lau WKO, Heng PWS, Bhuvaneswari R, Olivo M. Fluorescence imaging and phototoxicity effects of new formulation of chlorin e6–polyvinylpyrrolidone. J. Photochem.Photobiol. B. 2006;84:103-10.

[48] Gomer CJ, Razum NJ. ACUTE SKIN RESPONSE IN ALBINO MICE FOLLOWING PORPHYRIN PHOTOSENSITIZATION UNDER OXIC AND ANOXIC CONDITIONS.

Photochem. Photobiol. 1984;40:435-9.
[49] Homey B, von Schilling C, Blümel J, Schuppe H-C, Ruzicka T, Ahr HJ, et al. An Integrated Model for the Differentiation of Chemical-Induced Allergic and Irritant Skin Reactions. Toxicol. Appl. Pharm. 1998;153:83-94.

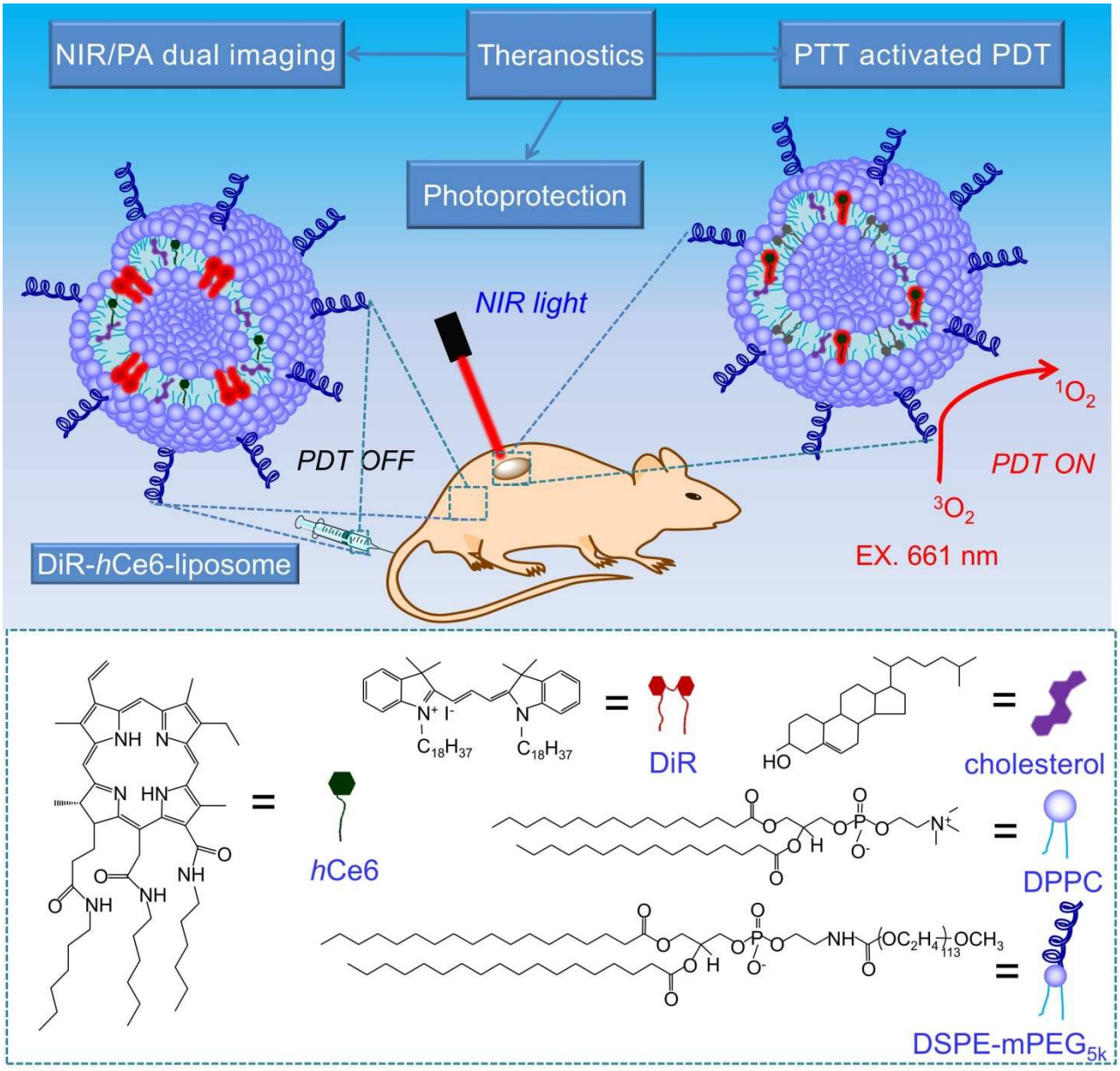

Figure 1. A scheme illustrating the chemical compositions of DiR-*h*Ce6-liposome and its applications for skin photo-protectable NIR light activated synergistic cancer phototherapy.

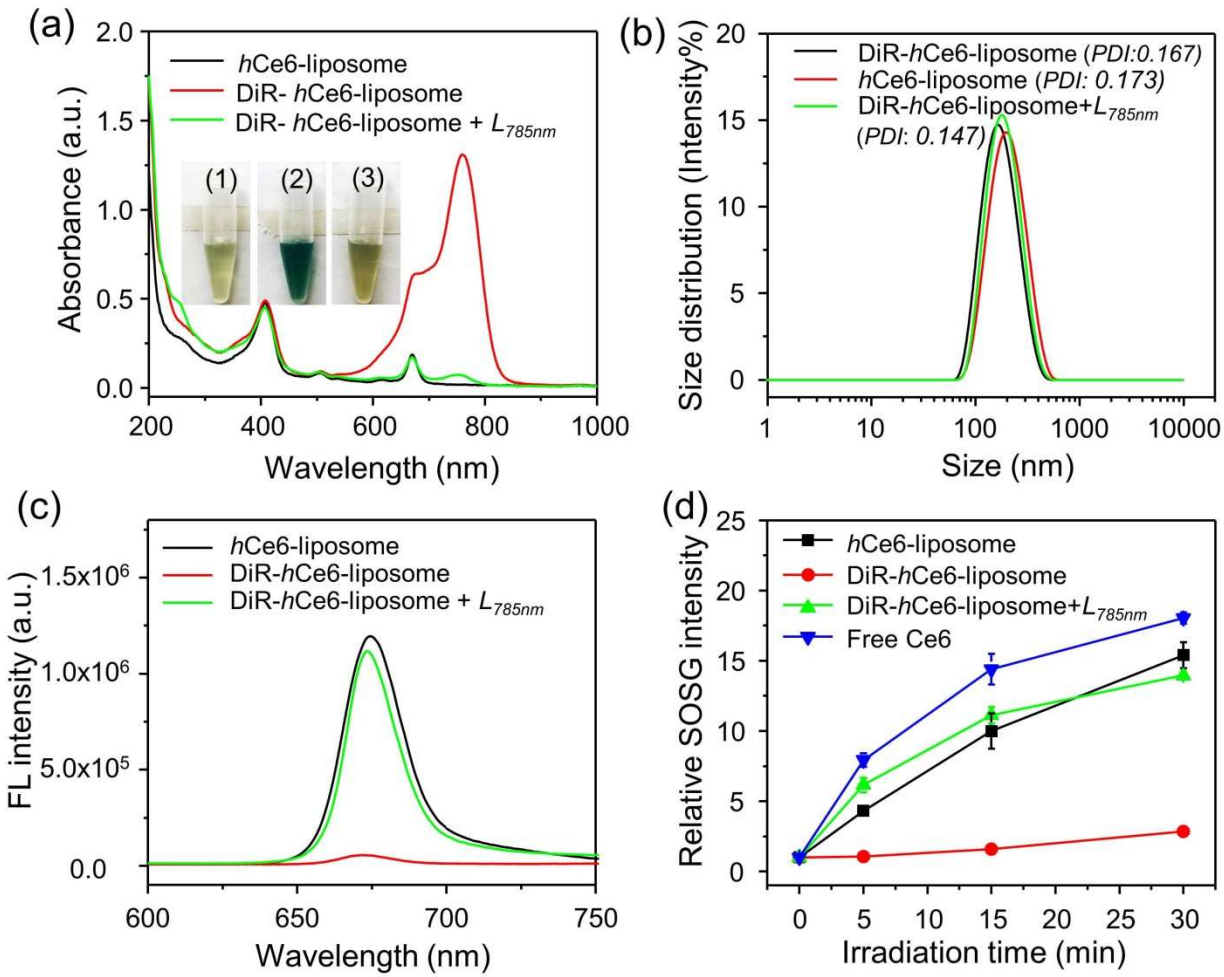

Figure 2. Effects of 785-nm laser irradiation on the optical, size distribution, and singlet oxygen generation profiles of DiR-*h*Ce6-liposome. (a-c) UV-vis-NIR absorbance spectra (a), DLS size distribution (b), and fluorescence spectra (c) of *h*Ce6-liposome (1), DiR-*h*Ce6-liposome (2), and DiR-*h*Ce6-liposome with a 785-nm laser irradiation (L_{785nm}) at 1 W cm^{-2} for 10 min (3). Inset in (a) shows digital photos of these three samples. (d) Singlet oxygen generation abilities of DiR-*h*Ce6-liposome with and without 785-nm laser irradiation as aforementioned, *h*Ce6-liposome, and free Ce6 determined by using a singlet oxygen sensor green (SOSG) kit. The concentration of Ce6 was 5 μM in those experiments. The error bars were based on triplicated measurements.

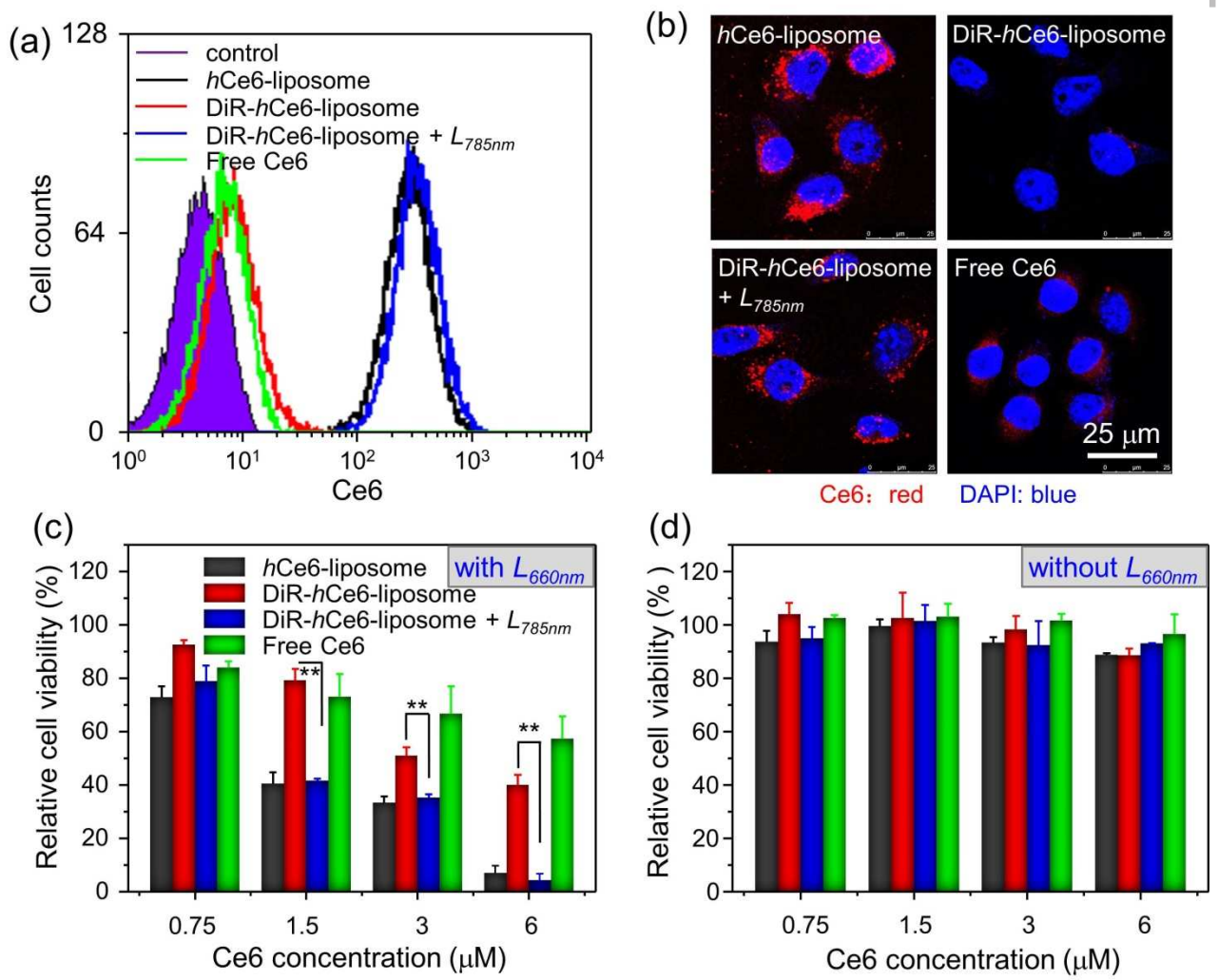

Figure 3. Intracellular internalization and cytotoxicity of DiR-*h*Ce6-liposome. (a&b) Flow cytometric analysis (a) and CLSM observation (b) of the intracellular internalization profiles of free Ce6, *h*Ce6-liposome, and DiR-*h*Ce6-liposome with and without a 785-nm laser pre-irradiation (L_{785nm}, 1 W cm^{-2} for 10 min) at the same Ce6 concentration. (c&d) Relative viabilities of 4T1 cells incubated with *h*Ce6-liposome, DiR-*h*Ce6-liposome, DiR-*h*Ce6-liposome + L_{785nm}, and free Ce6 for 2 h, then irradiated with (c) or without (d) a 660-nm LED light (L_{660nm}) for 15 min followed by additional 22 h incubation before the standard MTT assay. The error bars were based on triplicated measurements. *P* values were calculated by the Student's *t* -test: **P* < 0.05, ***P* < 0.01 (n = 3).

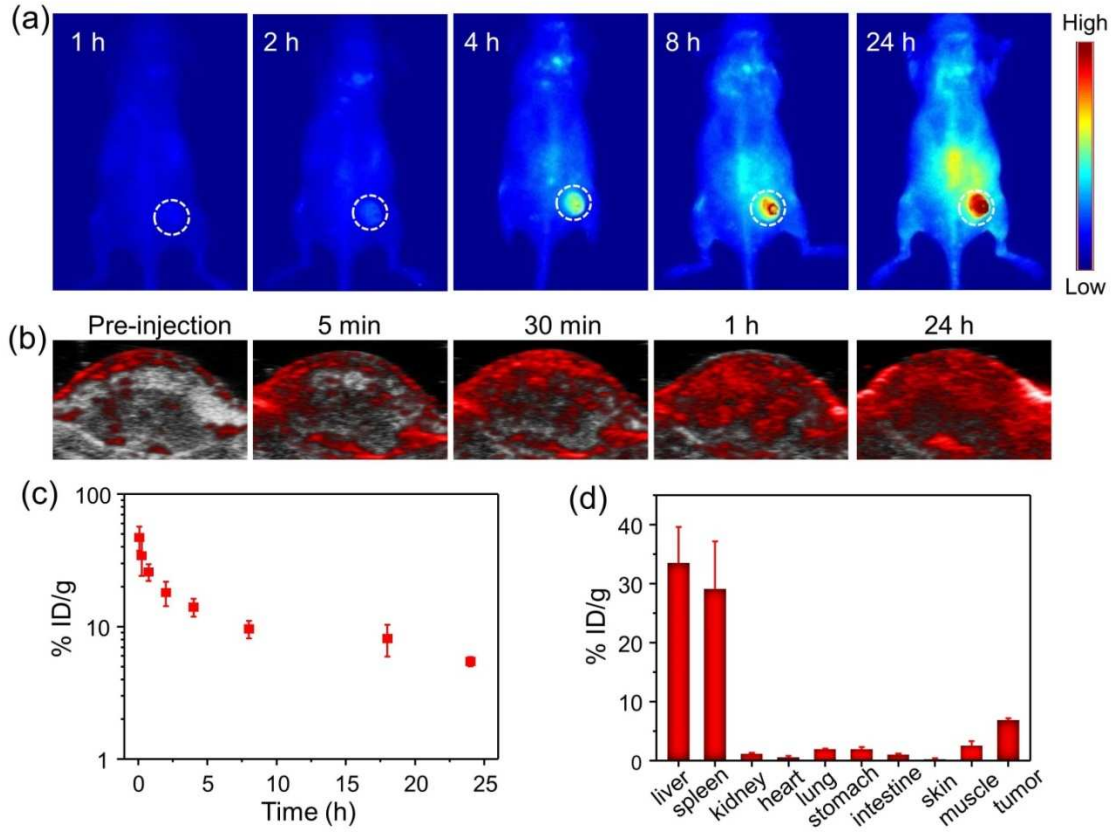

Figure 4. In vivo behaviors of DiR-*h*Ce6-liposome. (a&b) Time-lapsed in vivo NIR fluorescence (a) and PA (b) imaging of 4T1 tumor bearing mice. For NIR fluorescence imaging, the mice were imaged with an excitation at 735 nm, emission spectra within 780-950 nm, and exposure time of 100 ms. The tumor was indicated by white dashed circles in those fluorescence images. For PA imaging, ultrasound (gray) and photoacoustic (red) images were overlaid with one another. (c&d) In vivo blood circulation (c) and biodistribution (d) profiles of DiR-*h*Ce6-liposome in 4T1 tumor-bearing mice. The data were obtained by recording the fluorescence of DiR in all samples. Error bars were based on triplicated measurements.

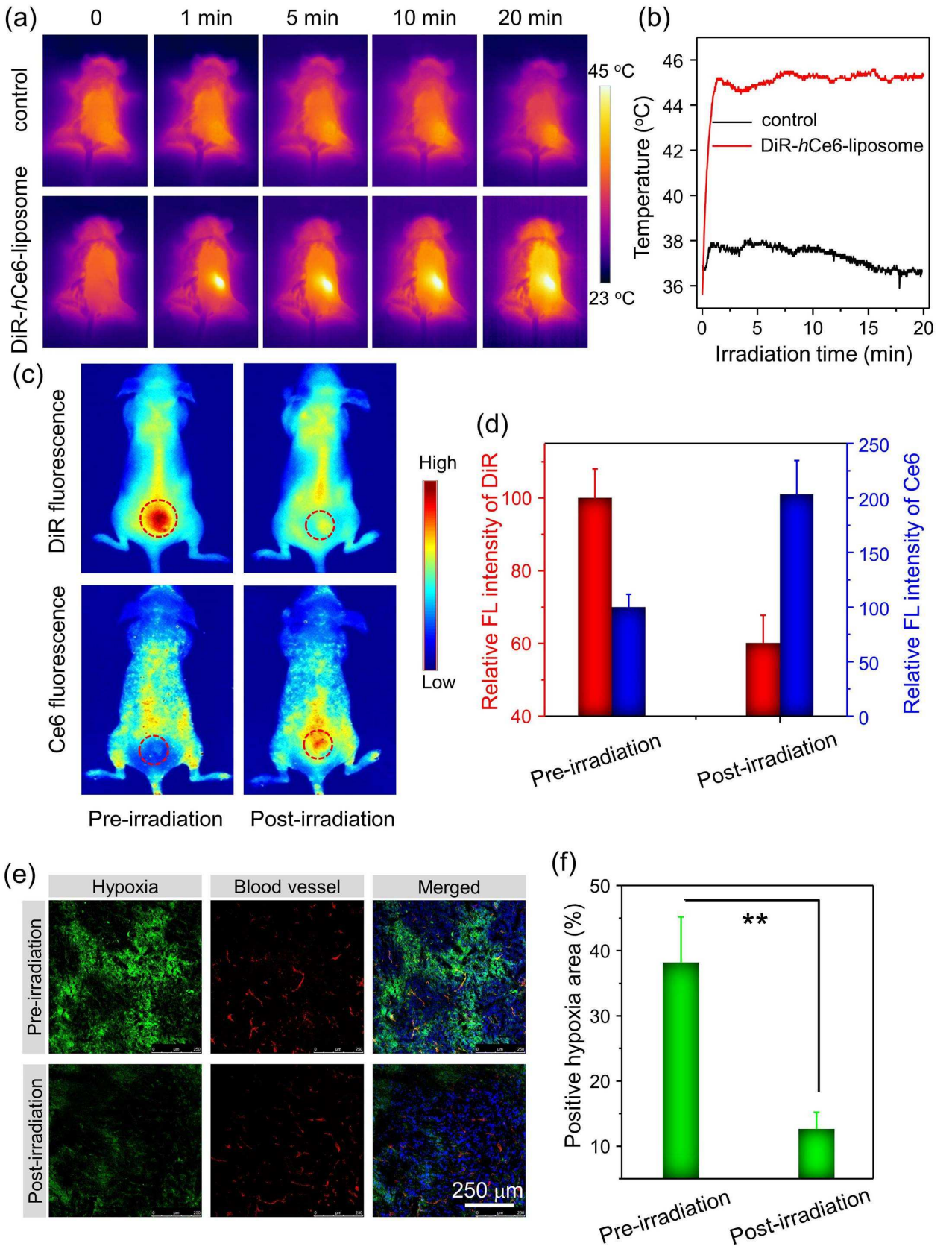

Figure 5. In vivo activation of DiR-*h*Ce6-liposome by NIR laser irradiation and the followed tumor oxygenation. 4T1 tumor bearing mice with an i.v. injection of DiR-*h*Ce6-liposome were exposed to a 785-nm laser at ~0.7 W cm^{-2} for 20 min. (a&b) In vivo infrared thermal imaging (a) and the corresponding tumor temperature change curves (b) recorded using an infrared thermal camera. (c)

In vivo DiR fluorescence bleaching (upper panel) and *h*Ce6 fluorescence recovery (down panel) as imaged by the Maestro in vivo optical imaging system. The excitation and emission wavelengths for DiR and *h*Ce6 fluorescence imaging were 735 nm / 800 nm and 523 nm / 660 nm, respectively. Tumors were highlighted using the red dashed circles. (d) Relative fluorescence (FL) intensity of DiR and *h*Ce6 at emission wavelengths of 800 nm and 660 nm, respectively, based on the in vivo images shown in (c). (e) Immunofluorescence staining of tumor slices from DiR-*h*Ce6-liposome injected mice before and after 785-nm laser treatment of their tumors. Tumor hypoxic regions, blood vessels and nuclei were shown in green, red and blue, respectively. (f) Semi-quantitative analysis of the percentage of positive hypoxia region before and after laser irradiation based on the images shown in (e). *P* values were calculated by the Student's *t* -test: $*P < 0.05$, $**P < 0.01$ (n = 3).

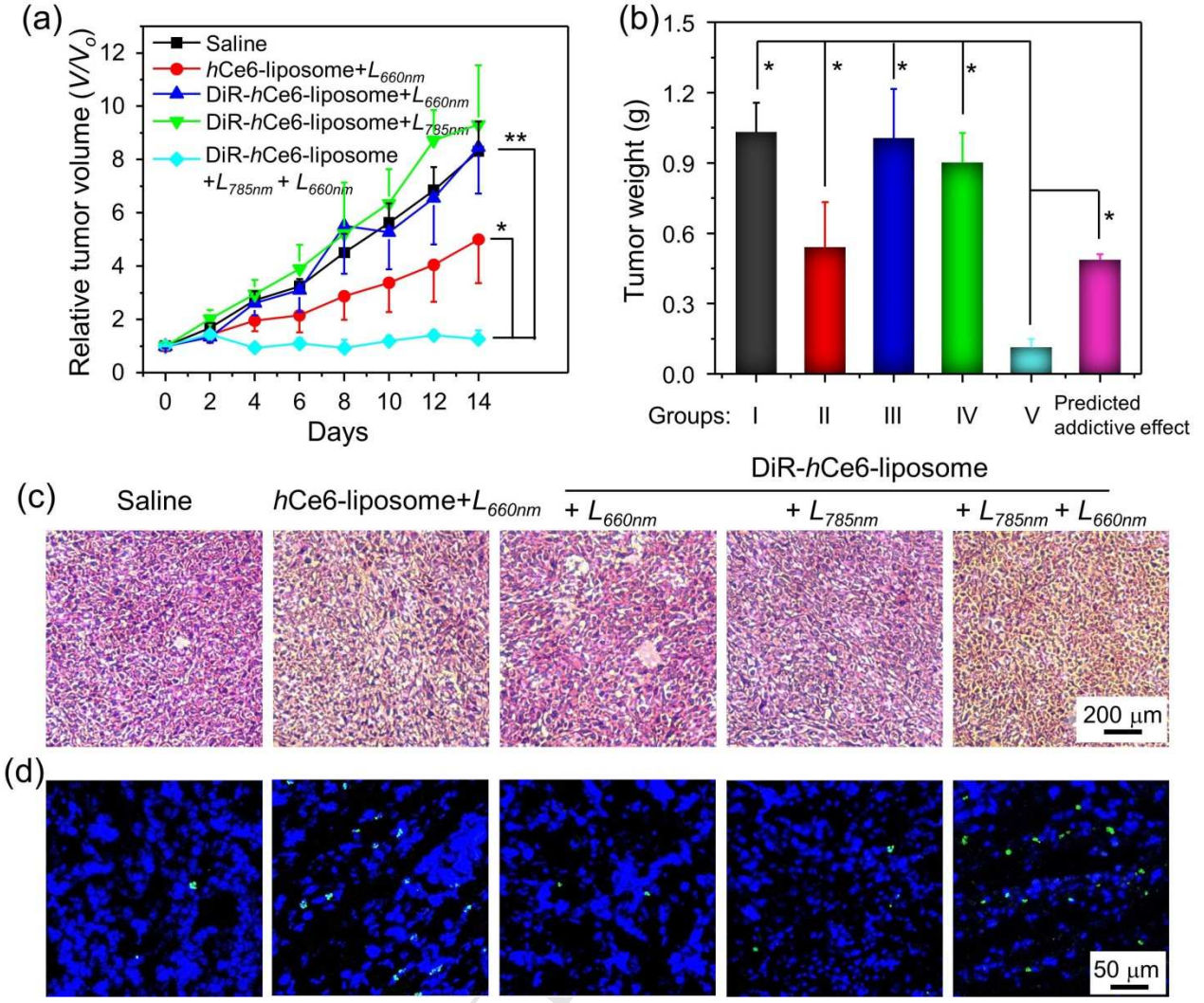

Figure 6. In vivo NIR light activated synergistic cancer phototherapy. (a) Relative tumor volume (V/V_o) changing curves of mice after various different treatments at indicated for 14 days. V and V_o stood for the tumor volumes after and before the treatment, respectively. Error bars were based on five mice in each group. P values were calculated by the Student's t -test: $^*P < 0.05$, $^{**}P < 0.01$ (n = 5). (b) Average tumor weight of tumors collected from different groups 14 d after the treatment. Groups I, II, III, IV, and V was used to stand for the group of saline (control), *h*Ce6-liposome + L_{660nm} (conventional PDT), DiR-*h*Ce6-liposome + L_{660nm} (quenched PDT), DiR-*h*Ce6-liposome + L_{785nm} (PTT alone), and DiR-*h*Ce6-liposome + L_{785nm} + L_{660nm} (activated PDT) in (a&b), respectively. The predicted addictive effect was calculated by multiplying the tumor growth inhibition ratios of group II and group IV. The dose of Ce6 was 3.5 mg kg^{-1}. L_{660nm} and L_{785nm} stand for 660-nm LED light irradiation at 2 mW cm^{-2} for 1 h and 785-nm laser irradiation at ~0.7 W cm^{-2} for 20 min, respectively. (c&d) H&E (c) and TUNEL staining (d) of tumor slices collected from mice from various groups at 24 h post laser irradiation.

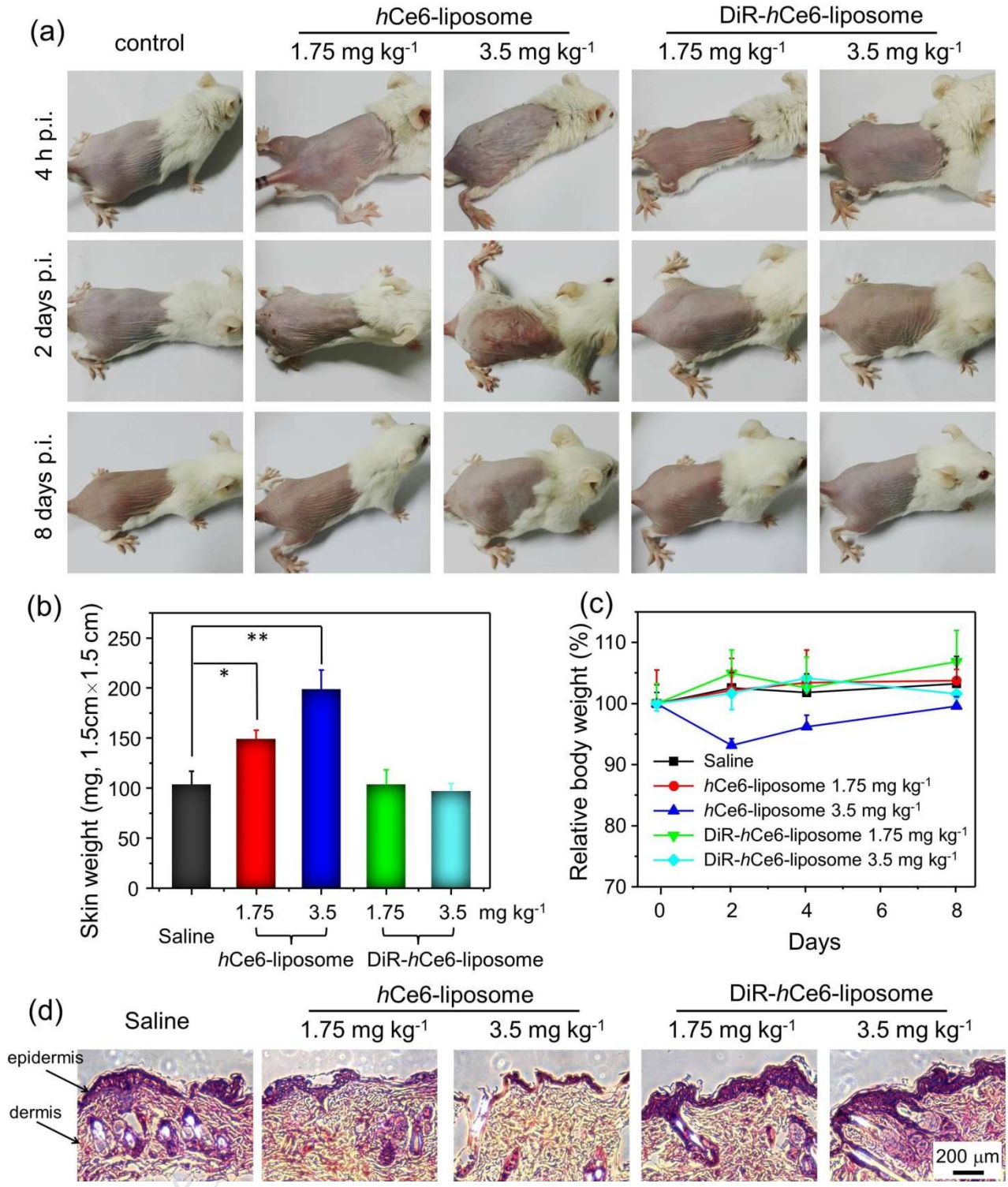

Figure 7. In vivo photo-toxicity of DiR-*h*Ce6-liposome and *h*Ce6-liposome to mouse skin. (a) Digital photographs of mice after various treatments as indicated at 4 h, 2 days, and 8 days post a 660-nm LED light exposure of 2 mW cm^{-2} for 30 min. (b) Weights of skins with a fixed size at 1.5 cm × 1.5 cm collected from the sacrificed mice at 4 h post laser irradiation. The error bars were based on 3 mice in each group. *P* values were calculated by the Student's *t* -test: $*P < 0.05$, $**P < 0.01$ (n = 3). (c) Relative body weight changing curves within 8 days post irradiation. The error bars were based on 5 mice in each group. (d) Micrographs of H&E stained skins of various groups collected at 2-days post irradiation.